Environmental Science Advances

ROYAL SOCIETY OF CHEMISTRY

PAPER

View Article Online
View Journal | View Issue

Cite this: *Environ. Sci.: Adv.*, 2022, **1**, 849

Green synthesis of SrO nanoparticles using leaf extract of *Albizia julibrissin* and its recyclable photocatalytic activity: an eco-friendly approach for treatment of industrial wastewater

Annin K. Shimi,[a] C. Parvathiraj,[a] Suman Kumari,[b] Jasvir Dalal, *[b] Vipan Kumar,[c] Saikh M. Wabaidur[d] and Zeid A. Alothman [d]

The present work unveils the reusable photocatalytic action of strontium oxide (SrO) nanoparticles synthesized using *Albizia julibrissin* plant extract *via* the co-precipitation method. The material and its synthesis reveal an eco-friendly approach that provides new insight into synthesizing the photocatalyst. The plant extract controls the parameters such as particle size, morphology, structure and other characteristic features of the synthesized material which are important aspects of a photocatalyst. The microscopy images of the as-synthesized SrO nanoparticles show that the particles exhibit spherical morphology with a rough surface and agglomeration of particles was also observed. The spherical morphology of SrO nanoparticles leads to a higher aspect ratio and assists in higher adsorption of pollutant dye. Using a Tauc plot, an energy bandgap of 2.64 eV is estimated for SrO nanoparticles, which is favorable for absorption of visible light. The synergic effect of structural and morphology parameters leads to an enhanced photo-degradation/pollutant removal efficiency of 87.4% for cationic methylene blue dye under visible light irradiation. In addition, the reusability of the SrO photocatalyst over four cycles is tested, and the results indicate that SrO can be proven to be an effective eco-friendly photocatalyst.

Received 30th January 2022
Accepted 6th September 2022

DOI: 10.1039/d2va00018k

rsc.li/esadvances

Environmental significance

In the last decade, the world has achieved a new height of success in the development of various nanotechnology areas such as sensors, biomedicines, food technology, electrochemistry, cosmetics, pharmaceuticals, catalysis, *etc.* However, these developments happen at the cost of environmental pollution, and still continue. It is either the synthesis of nano-materials using traditional methods or industrial development that generates huge amounts of gas/liquid/solid waste. Traditional methods produce unwanted and harmful by-products. To circumvent such issues, we reported the green synthesis of a SrO nanomaterial and tested it as a photocatalyst for the degradation of environmental pollutants under visible light. Thus, the work is environmentally friendly with no negative implications on the surrounding.

Introduction

In the last decade, the world has achieved a new height of success in the development of various nanotechnology areas such as sensors, biomedicine, food technology, electrochemistry, cosmetics, pharmaceuticals, catalysis, *etc.* However, these developments happen at the cost of environmental pollution,[1,2] and still continue. It is either the synthesis of nano-materials using traditional methods or industrial development that generates a huge amount of gas/liquid/solid waste. The traditional synthesis methods produce unwanted and harmful by-products. To circumvent such issues, green synthesis has attracted great attention owing to its reliable, economical, sustainable, and eco-friendly nature for processing various types of materials in this modern era of technology. Green synthesis plays a crucial role in the conservation of the environment by reducing the harmful effects of traditional synthesis methods employed in labs and industries such as paint, tannery, textiles, plastics, rubber, cosmetics, *etc.*[3–6] These industries use huge quantities of dyes, about 1.6 million tons yearly, which in turn results in the discharge of vast amounts of dye-laden effluent as sewage waste.[7] Industrial waste is a major factor of water pollution, wherein produced wastewater

[a]*Department of Physics, Manonmaniam Sundaranar University, Tirunelveli 627012, Tamil Nadu, India*

[b]*Department of Physics, Chaudhary Ranbir Singh University, Jind 126102, India. E-mail: jasvirdalal2012@gmail.com*

[c]*Department of Pharmaceutical Chemistry, JCDM College of Pharmacy, Sirsa 125055, India*

[d]*Department of Chemistry, College of Science, King Saud University, Riyadh 11451, Saudi Arabia*

contains various hazardous dyes such as rhodamine B, methyl-orange, methylene blue, *etc.* or contains heavy metal ions like Pb^{2+}, Hg^{2+}, Cr^{6+}, *etc.* whose highly toxic and poisonous nature causes serious diseases such as skin irritation, respiratory diseases, contact dermatitis, cancer, *etc.* in living beings that live on earth as well as in aquatic life.[8,9] Among the above-mentioned pollutant dyes, methylene blue is frequently used. Due to its heterocyclic chemical structure, the dye can sustain for a long time in the environment which causes harmful effects on human beings.[10] Thus, the elimination of by-products of traditional nanomaterials synthesis methods and removal of toxic pollutants from wastewater is the biggest challenge for humanity. Therefore, there is an urgent need for the establishment of a green synthesis method for nanomaterials and catalysts for the treatment of polluted water.

The treatment of polluted water can be performed *via* different ways such as adsorption, biodegradation, chlorination, ozonation, sedimentation, and chemical precipitation.[11–13] But these methods need an enormous amount of energy and chemicals. In recent years, semiconducting material-based photocatalysts have been introduced as a crucial green technology to eliminate environmental pollution problems.[14,15] The irradiation of semiconductors causes the generation of electron and hole (e–h) pairs which exhibit oxidation and reduction capabilities. The photo-generated charge carriers act directly or create other active radical species in the pollutant which decomposes it into organic/inorganic molecules *via* oxidation/reduction reaction.[16–18] For the technological purpose of photocatalysts, the dominant factors include higher photocatalytic efficiency, lower degradation time, quantity of catalyst, reusability, reproducibility of results, type of light, cost, *etc.* However, most photocatalysts failed to meet the above-mentioned criteria.[19–21]

Metal oxide nanoparticles such as CuO, MgO, CeO_2, SnO_2, TiO_2, ZnO and WO_3 are broadly used for photocatalysis, which is due to their high stability, appropriate energy bandgap, ion production, free radical generation and enhanced e–h pair lifetime properties.[22–26] Their non-toxic nature in water, abundance, cost-effectiveness and sustainability in various environmental fields make metal oxides suitable candidates for photocatalysts.[27] Among the metal oxides, SrO can be used for biomedical, cancer therapy, sensor, supercapacitor and catalyst applications. It is also applicable in dentistry, bone tissue treatment and biodiesel production. Recently, SrO has proven suitable for photocatalysis owing to its higher flexibility, chemical stability, suitable energy bandgap, crystal structure, *etc.*[28] The green synthesis route can control the structural and morphological features of materials. It is also reported that the materials synthesized *via* the green synthesis method have higher reactivity and aspect ratio than the materials synthesized *via* the traditional chemical method.[29]

Plant extracts are preferred over other synthetic chemicals because they are readily available and safe to handle, and have a wide range of metabolites. *Albizia julibrissin* belongs to the family Fabaceae and is also known as the silk tree, powder-puff tree, or mimosa. It is found in Africa, Asia, Australia, and tropical and subtropical regions of the Americas. It contains a wide range of phytoconstituents including flavonoids, glycosides, saponins, lignans, furans and fatty acids, and triacylglycerol has been identified in this plant.[30,31] These phytochemicals can act as reducing agents as well as capping agents. Nevertheless, little literature is available on the green synthesis of SrO nanoparticles, using extracts from plants including *Ocimum sanctum*, *Vintis vinifera* and *Elodea Canadensis*.[29,32,33]

The present work emphasizes the importance of the green synthesis method using *Albizia julibrissin* plant extract and the photocatalytic activity of plant extract mediated SrO nanoparticles. The plant extract acts as a capping and stabilizing agent that controls the characteristics of SrO nanoparticles, as analyzed using various techniques. The photocatalytic response of SrO nanoparticles is examined for the degradation of water pollutant methylene blue dye under irradiation with visible light. This work provides a significant understanding of the unique properties of SrO nanoparticles synthesized *via* the green method coupled with photocatalytic technological application.

Experimental details

Materials used and synthesis of SrO nanoparticles

Analytical grade strontium nitrate hexahydrate ($Sr(NO_3)_2 \cdot 6H_2O$), sodium hydroxide (NaOH), hydrochloric acid (HCl), and natural extract of *Albizia julibrissin* were used for the synthesis of SrO samples.

Albizia julibrissin plants have a wide range of biomolecules and metabolites, including vitamins, proteins, coenzyme-based intermediates, flavonoids, phenols, and carbohydrates.[30,31] Carbonyl, hydroxyl, and amino functional groups in such plant compounds interact with metal ions to reduce their particle size to the nanoscale. Flavonoids include a variety of functional groups, but the –OH group is thought to be the most important for changing metal ions to NPs.[34] These compounds also play a critical role in the capping of nanoparticles, which is critical for stability and biocompatibility.[35] It is reported that flavonoids and phenolic chemicals found in the extract are expected to be responsible for the conversion of metal ions to metal oxide nanoparticles.[36]

For the preparation of the extract, clean *Albizia julibrissin* leaves were boiled in 100 mL double distilled water for 10 min, and filtered using Whatman filter paper. The extract was stored in a refrigerator at 4 °C. For the synthesis of SrO nanoparticles, 0.1 M $Sr(NO_3)_2 \cdot 6H_2O$ was mixed into 10 mL of plant extract solution using a magnetic stirrer for 1 hour at 60 °C and the color of the solution turned to a greenish color. Afterward, the solution was centrifuged, washed and dried in a hot air oven at 90 °C. Finally, the dried sample was collected and crushed into powder for further analysis. Scheme 1 shows the schematic illustration of the preparation process for SrO nanoparticles (SrO NPs).

Characterization techniques

The bio-synthesized SrO nanoparticles were characterized to investigate their structural, elemental and morphological

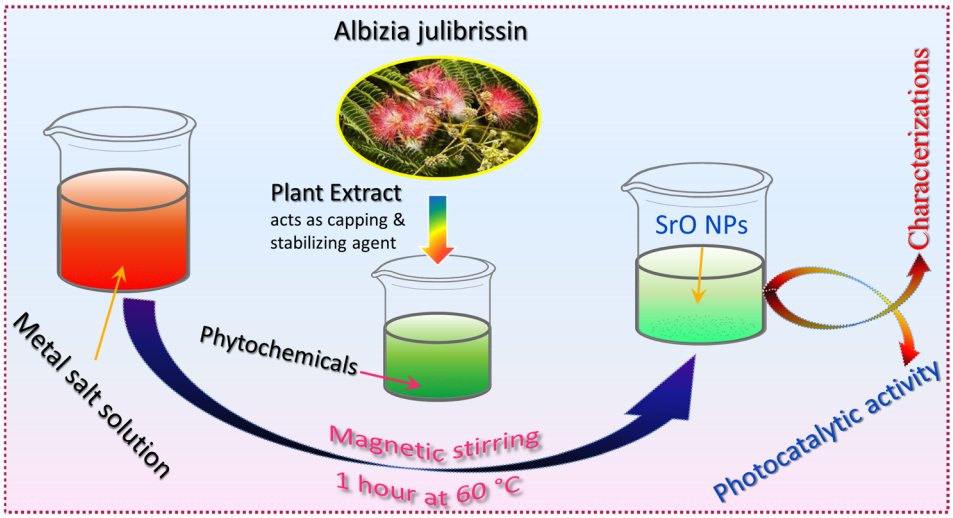

Scheme 1 Schematic illustration of the green synthesis procedure for SrO nanoparticles.

properties. The structural configuration of SrO NPs was identified using a Malvern Panalytical X-ray diffractometer (XRD) operated at 25 mA and 40 kV (Cu Kα radiation with $\lambda = 1.5406$ Å). The morphological properties were investigated using a Carl Zeiss Field Emission Scanning Electron Microscope (FESEM) with Energy Dispersive X-ray (EDX) spectroscopy at an accelerating voltage of 15 kV and a Philips CM200 Transmission Electron Microscope (TEM) at an accelerating voltage of 200 kV. The binding energies between the nanoparticles were examined using X-ray Photoelectron Spectroscopy (XPS, PHI 5000 Versa Probe III, Physical Electronics, USA). The functional groups and chemical bonds of the samples were studied with a Fourier Transform Infrared (FTIR) PerkinElmer instrument (4000–400 cm^{-1}) using KBr pellets. The UV-diffuse reflection spectra (UV-DRS) of the as-prepared samples were recorded on a UV-2600 Shimadzu spectrometer.

Photocatalytic activity

The photocatalytic activity of *Albizia julibrissin* facilitated SrO nanoparticles was tested against methylene blue (MB) dye under visible light irradiation. For this purpose, the SrO catalyst was added to a polluted water sample (containing 10 ppm MB molecules) and placed under dark conditions for 20 min to reach the adsorption–desorption equilibrium. After that, the dark-conditioned samples were taken out and kept directly under a visible light source (xenon lamp; power = 150 W & λ = 400 nm). The solution was irradiated for 80 min, and during this process at regular time intervals of 20 min, a test sample was collected from the solution. The collected samples were centrifuged to remove the SrO catalyst from the solution. The degradation efficiency was calculated from the UV-Vis spectra using eqn (1):

$$\text{Dye degradation efficiency } (\%) = \frac{C_0 - C_t}{C_0} \times 100 \quad (1)$$

where C_0 is the initial concentration of the MB dye solution without irradiation with light and C_t is the concentration of the dye solution at different time intervals upon irradiation with visible light. To ensure the accuracy of degradation efficiency, the experiment was repeated three times under similar conditions.

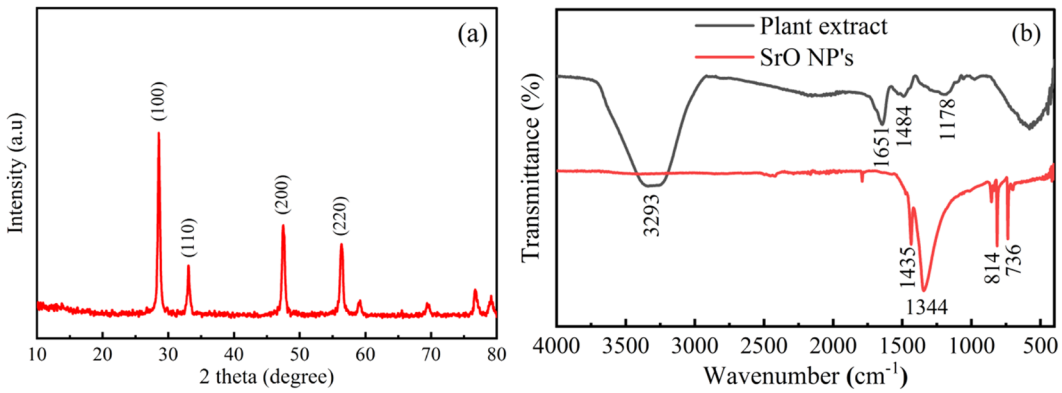

Fig. 1 (a) X-ray diffraction pattern of biosynthesized SrO NPs. (b) FTIR spectra of *Albizia julibrissin* extract and SrO NPs.

Results and discussion

XRD analysis

The crystal structure and phase of the prepared sample have been analyzed using XRD analysis. The XRD pattern of the sample is shown in Fig. 1a. The peaks observed in the as-prepared sample are positioned at 2θ values of 28.8, 33.3, 47.9 and 56.6° assigned to the planes (100), (110), (200) and (220) respectively. The obtained results impeccably match the standard face-centered cubic structure of SrO (JCPDS 48-1477). The formation of strong & sharp peaks and the absence of other peaks are indicative of the phase purity and crystalline properties of the synthesized material. Thus, the crystalline phase is indicative of a network of metal atoms and oxygen atoms. These

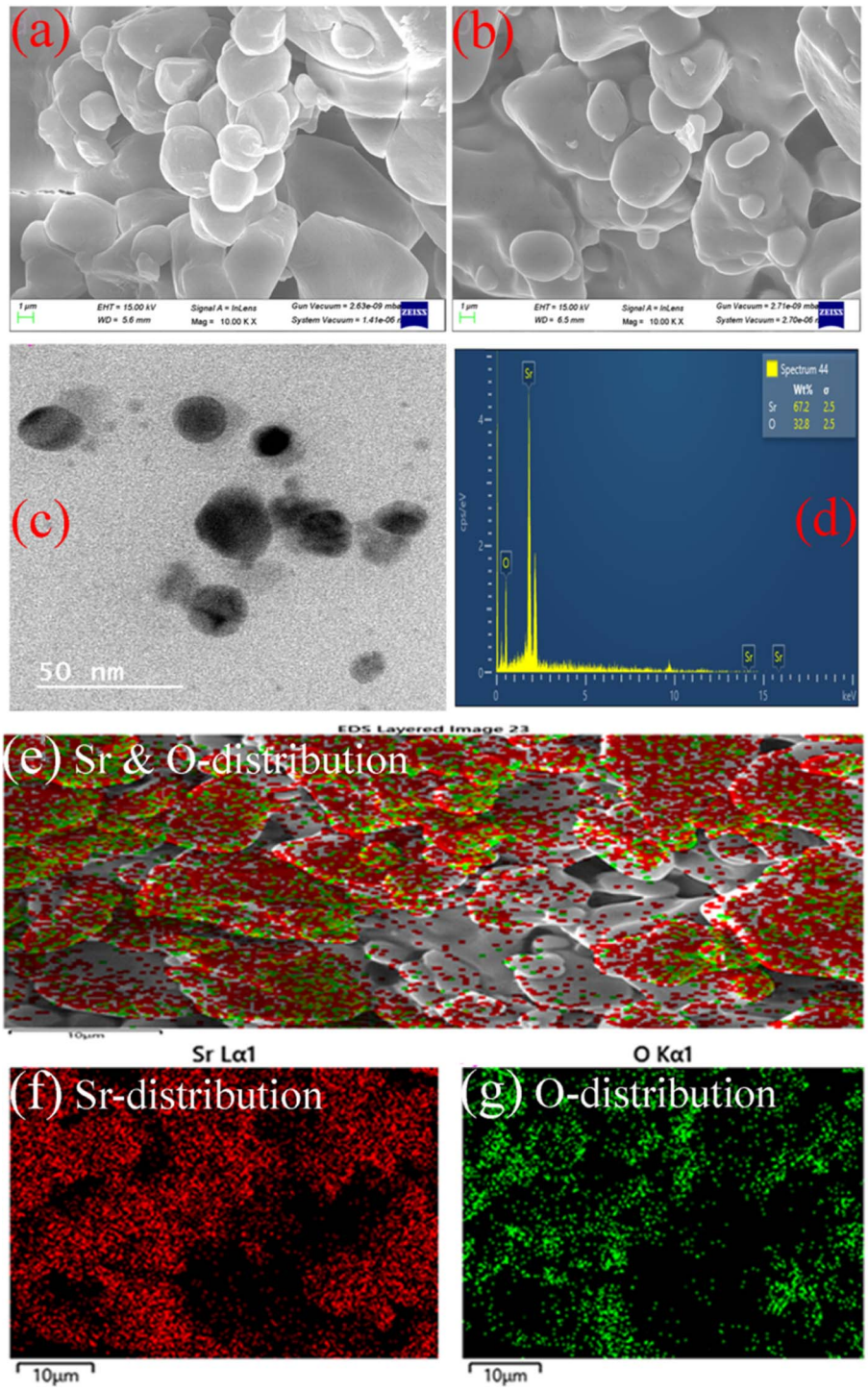

Fig. 2 (a and b) FE-SEM images of bio-synthesized SrO NPs, (c) TEM image of bio-synthesized SrO NPs, (d) EDX spectrum of SrO NPs. (e–g) Mapping images of synthesized SrO NPs.

parameters also reveal that the natural extract of *Albizia julibrissin* acts as a good stabilizing and capping agent. The average crystallite size (D) is calculated using the Debye–Scherrer equation as

$$D = \frac{K\lambda}{\beta \cos\theta} \quad (2)$$

where β is the full width at half maximum (FWHM), $K = 0.94$ (shape factor), $\lambda = 1.5405$ Å and θ is the diffraction angle. The average crystallite size of the sample is calculated at around 34 nm. It has been observed that a smaller crystallite size of the catalyst may be beneficial for the catalytic activity as compared to the bulk catalyst.[22]

FTIR analysis

FTIR spectroscopy is an advantageous technique to examine the chemical structure and functional group vibrations in the SrO sample and plant extract as depicted in Fig. 1b. The FTIR spectrum of the plant extract shows absorption bands at 3293, 1651, 1484, 1178, and 570 cm^{-1}. The broad peak at 3293 cm^{-1} indicates O–H stretching vibrations corresponding to water molecules.[37] The peak at 1651 cm^{-1} indicates the vibration of the C=O bond of the amide group.[38] The presence of a nitrile group, *i.e.* the C–N stretching vibration, is observed at 1484 cm^{-1}.[39] The peak observed at 1178 cm^{-1} can be attributed to C–C stretching and –OH distortion of primary alcohols and carboxylic acids.[36,40] The band centered at 570 cm^{-1} may be due to bending vibrations of aromatic compounds.

The absorption bands for *Albizia julibrissin* treated SrO NPs are observed at 1435, 1344, 814, and 736 cm^{-1}. The intense peaks located at 814 cm^{-1} and 736 cm^{-1} indicate the bending vibrations of the metal–oxygen bond which shows the formation of Sr–O.[41] A band at 1400–1000 cm^{-1} corresponds to methylene groups of proteins present in plant extract.[36] The bands positioned at 1435 and 1344 cm^{-1} reveal the presence of the metabolites and biomolecules of the *Albizia julibrissin* plant extract. It is reported that the free NH_2 and carbonyl groups from proteins have a tendency to form a layer over the particles that in turn stabilizes the nanoparticles.[36] Thus, the spectrum reveals that protein molecules, as well as flavonoids and their functional groups, assist the formation of strontium oxide and stabilize it *via* the capping of nanoparticles. As result, these elements play a vital role in the morphology and dispersity of nanoparticles.

Morphological and elemental analysis

The morphology and elemental details of *Albizia julibrissin* plant extract treated SrO nanoparticles have been examined using FESEM, TEM and EDX as presented in Fig. 2. FESEM is one of the best techniques to investigate the morphology of materials. The FESEM images show globular structures of different sizes (average size is ~5 μm) and with a rough surface as shown in Fig. 2a and b. The globular structure shows the agglomeration of SrO NPs. The accumulation of SrO NPs may be due to higher surface area and higher surface energy of the nanoparticles. From the TEM image (Fig. 2c), it has been observed that the particles appear to be of spherical shape and are distributed non-uniformly. The size of SrO nanoparticles is found to vary in the range of 20–30 nm; this obtained particle

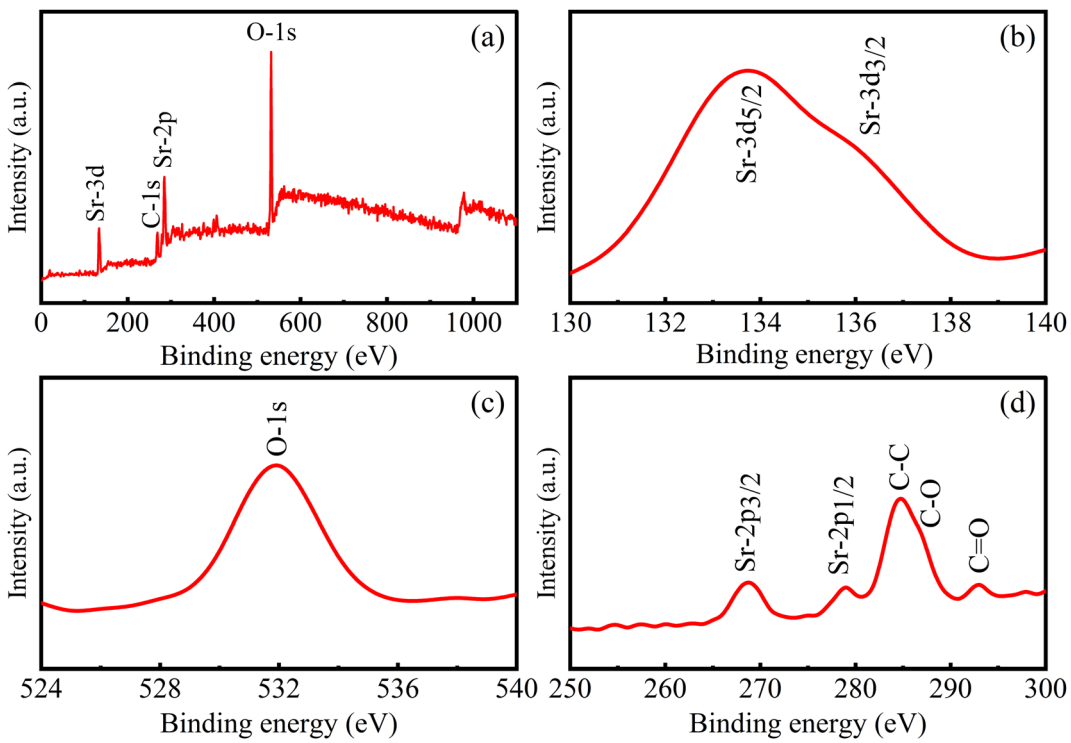

Fig. 3 XPS spectra of biosynthesized SrO NPs: (a) wide spectrum, (b) Sr-3d, (c) O-1s, and (d) core level Sr-2p & C-1s.

size is in close agreement with the crystallite size calculated from the XRD analysis. The particles have a spherical geometry which leads to higher surface area than other geometries, *i.e.* the particles' higher aspect ratio plays a crucial role in catalytic activity. Thus, these properties such as lower particle size, and spherical shapes with rough surfaces assist the adsorption of the dye molecule on the surface of SrO nanoparticles and the adsorption of dye is another vital parameter for enhanced photocatalytic activity.

Moreover, the formation of SrO NPs has been investigated through elemental analysis using energy-dispersive X-ray spectroscopy as shown in Fig. 2d–g. The presence of oxygen and strontium elements is visible at 0.52 and 1.86 keV respectively.[42] The contribution by weight of strontium and oxygen in the total particle weight is found to be 67.2% and 32.8% respectively. The elemental color mapping of the sample is depicted in Fig. 2e–g, and confirms that both elements, *i.e.* strontium and oxygen elements, are present in the biosynthesized SrO NPs. And no other impurity has been observed from the figures. Thus, the results confirmed the formation of SrO NPs of good quality and confirmed that the present biosynthesis process using plant extract has wide scope to synthesize other such materials *via* an eco-friendly route. This will be useful for environmental safety as well as the synthesis of high quality materials.

Evaluation of binding energy

The chemical nature of the elements existing in the as-synthesized sample can be investigated using a quantitative X-ray photoelectron spectroscopy technique (XPS). The spectra can be obtained by measuring electron number and kinetic energy simultaneously during irradiation of the material with an X-ray beam.[43] The composition of the sample has also been analyzed from a detailed investigation of the XPS spectra of Sr-3d, Sr-2p, O-1s, and C-1s as depicted in Fig. 3. As observed from the figure, peaks corresponding to binding energies 133.7 and 136.2 eV are assigned to Sr-$3d_{5/2}$ and Sr-$3d_{3/2}$ respectively due to spin–orbit coupling with separation of 2.5 eV.[44] In addition, the Sr-3p state is also split into two levels, Sr-$2p_{3/2}$ and Sr-$2p_{1/2}$ corresponding to binding energies 268.6 and 279 eV respectively, with the core spin–orbit coupling separation of 10.4 eV.[45] It is reported that these specific values of binding energy can be ascribed to the Sr^{2+} ionic state in the as-prepared SrO sample.[42] In addition, the intense peak at 531 eV (Fig. 3c) indicates the existence of the O-1s orbital level and is assigned to lattice oxygen with an O^{2-} oxidation state.[46] In the C-1s spectrum, three specific peaks associated with C–C/C=C, C–O and C=O are centered at 284.7, 286.9 and 292.5 eV respectively.[46] The peak corresponding to C–C bonds indicates that the plant extract is dispersed on the surface of nanoparticles. Thus, the plant extract acts as a capping agent on the surface of SrO, due to which the morphology of the nanoparticles may be spherical, and controls the dispersion as observed in the TEM micrograph. The plant phytochemicals such as flavonoids, saponins and tannins may be the main active species that give rise to the formation of SrO nanoparticles in a controlled manner. The obtained results for the synthesized SrO nanoparticles supported the FTIR findings that the plant metabolites are responsible for the formation and stabilization of the nanoparticles.

UV-DRS analysis

The optical properties have an important role in the investigation of the photocatalytic activity of a material. As per the theory of UV spectroscopy, the valence electrons of atoms are excited to a higher energy level *via* absorbing radiation energy. As a result of optical adsorption, a spectrum is obtained and from the analysis of the spectrum, the energy band-gap of the material can be assessed. This method is authenticated for obtaining a precise value of the energy band-gap which depends upon the delocalization of orbitals. The UV-DRS spectrum of the SrO nanoparticles is shown in Fig. 4a. The spectrum shows a broad absorption band positioned at around 300 nm. From the maximum absorption band, the energy band gap of the SrO nanoparticles has been calculated using Tauc's equation as:[47]

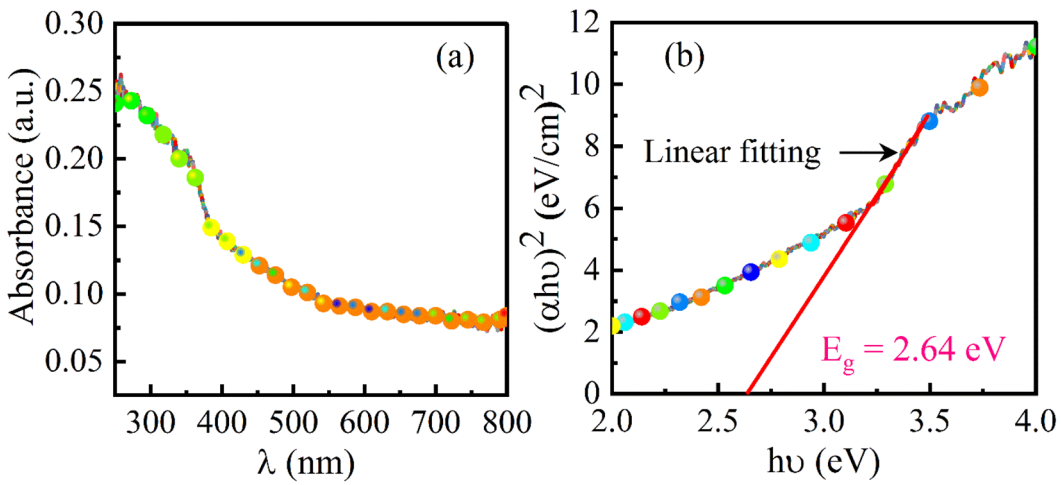

Fig. 4 (a) UV-DRS spectrum of biosynthesized SrO NPs and (b) Tauc plot of SrO NPs.

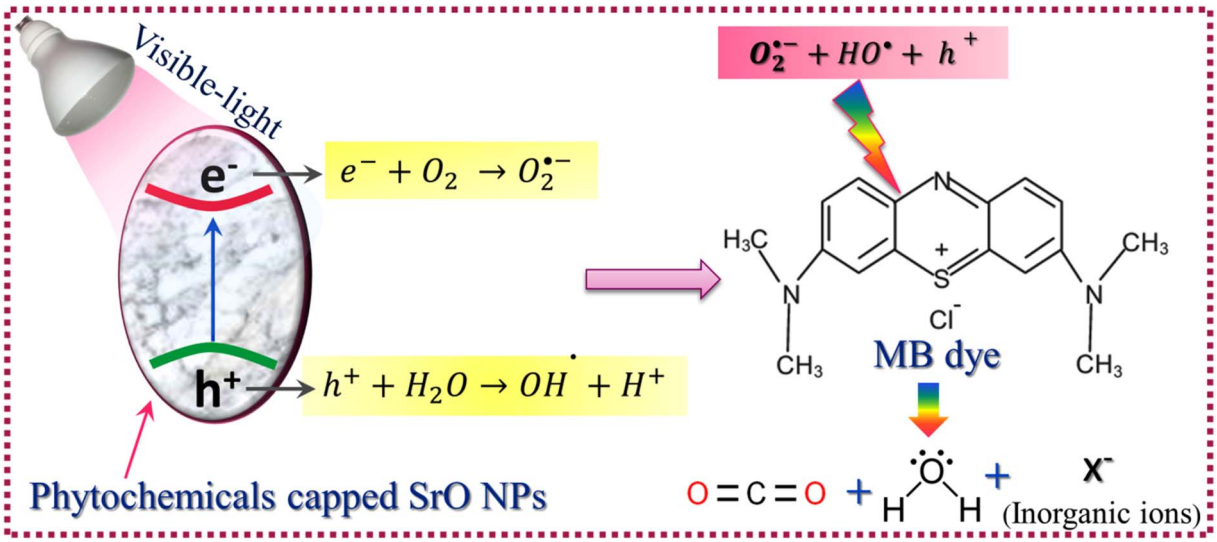

Scheme 2 Schematic illustration of the photocatalytic mechanism.

$$(\alpha hv)^n = A(hv - E_g) \quad (3)$$

where α, n, A, E_g, and hv are the absorption coefficient, power factor (its value is 2 for direct allowed transitions), intrinsic constant, band-gap of the catalyst and photon energy respectively. A plot of $(\alpha hv)^2$ *versus* hv was drawn and the linear fit was extrapolated to the *x*-axis as shown in Fig. 4b. From the extrapolated curve, the energy band-gap of SrO nanoparticles is found to be 2.64 eV which is higher than the energy band-gap of bulk SrO (1.8 eV).[48] According to the quantum confinement effect, a decrease in particle size is directly proportional to an increase in energy band-gap. The band-gap plays a vital role in dye degradation activity by producing free radicals that enhance catalytic activity.

Photocatalytic activity

For ease of understanding the obtained results, a potential photocatalytic mechanism for the degradation of MB dye under visible-light irradiation has been proposed as:

$$SrO + hv \rightarrow SrO(e^- \ \& \ h^+) \text{ (formation of EHPs)} \quad (4)$$

$$e^- + O_2 \rightarrow O_2^{\bullet -} \text{ (formation of superoxide anionic radical)} \quad (5)$$

$$h^+ + H_2O \rightarrow OH^{\bullet} + H^+ \text{ (formation of hydroxyl radical)} \quad (6)$$

$$O_2^{\bullet -} + 2H^+ + e^- \rightarrow H_2O_2 \text{ (formation of hydrogen peroxide)} \quad (7)$$

$$(H_2O_2 + O_2^{\bullet -} + OH^{\bullet}) + C_{16}H_{18}ClN_3S \text{ (MB)} \rightarrow CO_2 + H_2O + NO_3^- + NH_4^+ + Cl^- \quad (8)$$

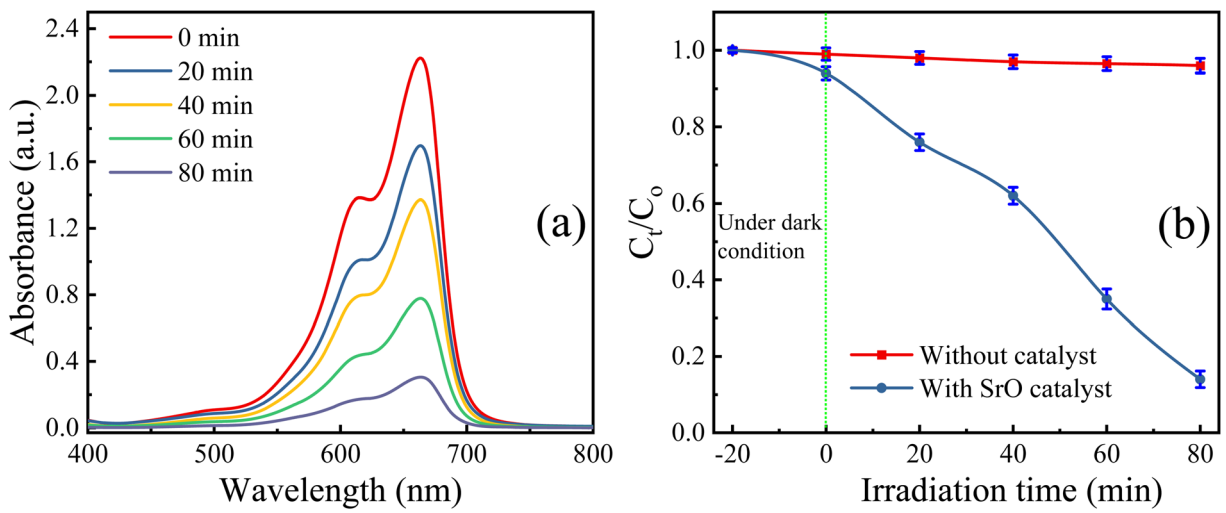

Fig. 5 (a) UV-DRS spectra of the test reaction (with SrO NPs) at different time intervals of visible light irradiation, and (b) variation in C_t/C_0 with irradiation time.

The SrO nanoparticles absorb visible light during the irradiation time span, resulting in the generation of electron–hole pairs (EHPs) inside the nanoparticles. Then some of the generated charge carriers are compensated through recombination and some of them migrate to the surface of the nanoparticles, where the electrons and holes contribute to the initiation of reduction and oxidation reactions respectively. The electrons involved in the reduction reaction with oxygen molecules result in the creation of superoxide anionic radicals and, furthermore, the superoxide anion produces the hydrogen peroxide species. The holes create hydroxyl radicals by oxidizing water molecules. The superoxide anion, hydrogen peroxide, and hydroxyl radicals are highly active species having the tendency to break the carbon–hydrogen bonds along with the carbon–carbon bonds of MB molecules that are adsorbed on the surface of the catalyst.[22] The reaction between active species and MB molecules results in the degradation of MB molecules into CO_2, H_2O, and some inorganic molecules such as NO_3^-, NH_4^+ and Cl^- as byproducts of the photo-catalytic reaction. The photocatalytic process is shown schematically in Scheme 2.

The SrO photocatalyst synthesized using the green synthesis approach has been tested for the degradation of methylene blue dye. MB dye is a virulent organic pollutant that is a major threat to the environment because of its huge use in industrial production. Therefore, MB has been chosen as an organic pollutant to assess the photocatalytic activity of as-synthesized SrO under visible light irradiation. The absorption intensity of MB aqueous solution in the presence of SrO nanoparticles at different time intervals on irradiation is shown in Fig. 5a. The characteristic absorption peak in the UV-DRS spectrum is found at 662 nm which was chosen for the measurement of the photocatalytic efficiency of the SrO nanoparticles by correlating the relative intensity of the peak with time. Fig. 5b shows the variation of the relative dye concentration (C_t/C_0) of MB dye in the aqueous solution as a function of time in the presence and absence of the photocatalyst. The decrease in the intensity of the peak as well as a decrease in the relative dye concentration of MB dye with time is due to damage of the chromophoric groups present in MB.[49,50] From the figure it appears that SrO exhibits an enhanced photocatalytic response with time, showing higher efficiency at a higher irradiation time. This is because a higher irradiation time generates a greater number of EHPs which produce a greater population of active species which enhances the degradation efficacy of the photocatalyst. The degradation of MB dye with the SrO photocatalyst reached 87.4% in 80 minutes, whereas, without the photocatalyst, the degradation was 4% in the same time interval.

Further, the photocatalytic response of the sample has been investigated quantitatively and more precisely through examination of the degradation kinetics of pollutant MB dye. The curves representing degradation in the relative concentration of MB dye *versus* irradiation time (Fig. 5b) are found to fit (R^2 = 0.97 (without catalyst) & 0.91 (with SrO catalyst)) an exponential decay curve well, indicating that the nature of the photocatalytic kinetics is consistent with a pseudo-first-order reaction as shown in Fig. 6a. The degradation rate constant of the pollutant dye has been calculated using eqn (9)[51]

$$-\ln\frac{C_t}{C_0} = kt \tag{9}$$

where k is the pseudo-first-order rate constant for the degradation of MB dye and t is the irradiation time. The rate constant has been calculated by assessing the slope of the $-\ln C_t/C_0$ curve plotted *versus* irradiation time (min).

The rate constant for the degradation of MB dye in the presence and absence of SrO nanoparticles has been calculated as 0.23 min^{-1} and 3 × 10^{-4} min^{-1}, respectively. The rate constant in the presence of SrO nanoparticles is much higher than that of the photolytic degradation reaction (without photocatalyst), which is consistent with the activity trends as observed in Fig. 5.

Effect of pH on the degradation of MB dye

The pH is a vital parameter in photocatalysis that can slow-down/speed up the degradation reaction, by controlling the surface charge properties of the catalyst resulting in an alteration in the adsorption efficiency of pollutants on the surface of the catalyst.[52,53] Therefore, the effect of pH on the degradation of

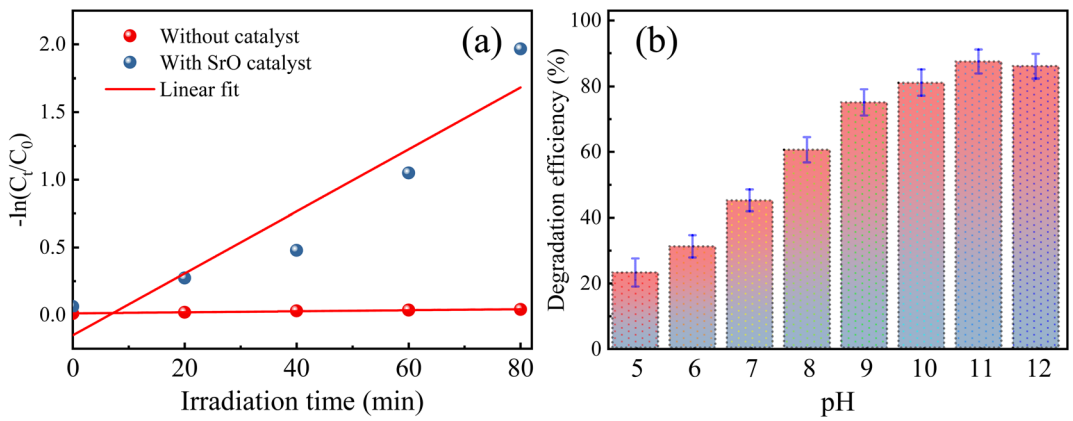

Fig. 6 (a) Kinetics of the degradation reaction for MB dye in the presence and absence of SrO nanoparticles and (b) effect of pH on the degradation of MB in the presence of SrO (irradiation time 80 min). Error bars indicate the % error in the repeated experiments.

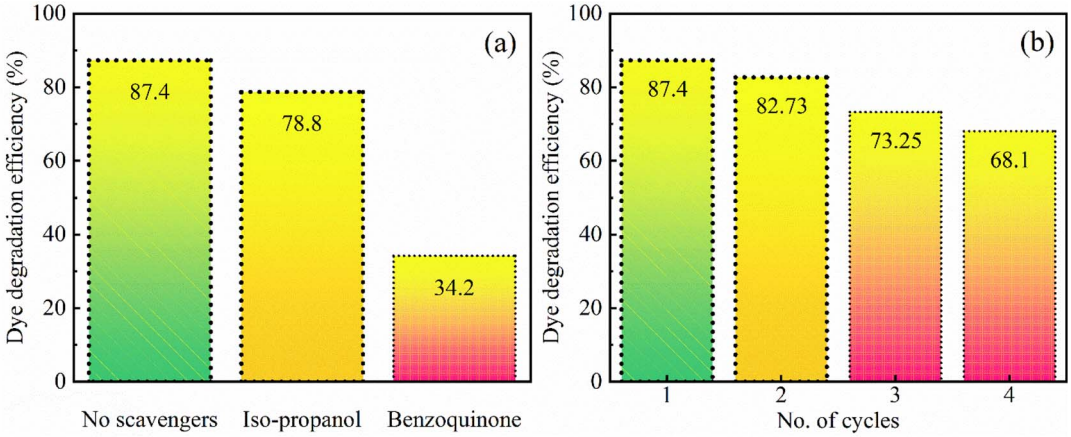

Fig. 7 (a) Dye degradation efficiency in the presence of scavengers and (b) reusability of the SrO sample under visible-light irradiation (irradiation time 80 min).

Table 1 Photocatalytic activity of metal oxides used for the photo-degradation of MB dye

Sr. No.	Metal oxide	Source of light	Power of source (W)	Degradation time (min)	Degradation (%)	References
1	SnO_2 NPs	UV-Vis	9	180	79	56
2	ZnO NPs	Visible light	20–40	180	82.1	57
3	ZnO nanoflowers	UV-Vis	300	60	83	58
4	ZnO NPs	UV-Vis	—	90	83.45	59
5	MgO NPs	UV-Vis	10	250	81	60
6	CuO NPs	Sunlight	—	300	80.71	61
7	ZnO NPs	UV-Vis	—	180	74	62
8	SnO_2 nanorods	UV-Vis	900	100	85	63
9	MgO	UV-Vis	160	150	64	64
10	SrO	Visible light	150	80	87.4	Present work

MB dye has been studied/optimized in the presence of the SrO photocatalyst in the range of 5–12. The pH level was controlled using hydrochloric acid and sodium hydroxide solution. The pH value of the solution was fixed once at the onset of irradiation of the solution; it was not measured during the reaction. Fig. 6b depicts the photodegradation efficiency (%) of the SrO sample at different pH values for MB dye.

It is observed from the figure that the degradation efficiency is increased with an increase in the pH value of the sample up to pH 11; a further increase in pH leads to a decrease in the efficiency. The maximum efficiency at pH 11 is due to a balance of electrostatic attraction forces between the positively charged MB dye molecules and negatively charged catalyst which in turn enhanced the adsorption of MB pollutant molecules on the catalyst surface.[47] As the pH value is lowered from 11, the lessening of the photocatalytic response of SrO nanoparticles may be due to the weakening of electrostatic forces or may be due to the formation of a salt *via* the reaction with acid. In the case of cationic dyes, several authors have also reported a higher degradation efficiency of metal oxide nanoparticles in basic medium.[54,55]

Radical scavenging

A radical scavenging experiment has been performed to understand the photocatalytic mechanism in more detail by identifying the most responsible radicals among the active species for the degradation of the pollutant dye. The $OH^{\bullet}$ and $O_2^{\bullet-}$ radicals are the two main possible species in the photodegradation of the pollutant dye. Iso-propanol and benzoquinone have been used as $OH^{\bullet}$ and $O_2^{\bullet-}$ radical scavengers respectively. With the addition of these chemicals, the photodegradation efficiency decreased as shown in Fig. 7. In the presence of iso-propanol, *i.e.* the $OH^{\bullet}$ radical scavenger, the degradation efficiency decreases to 78.8%, indicating that the $OH^{\bullet}$ radicals have a small contribution to the photocatalytic process. Moreover, the experiment was repeated in the presence of benzoquinone which is the most efficient electron acceptor due to its higher redox potential. Benzoquinone accepts electrons generated in SrO during the irradiation so that the $O_2^{\bullet-}$ radicals do not form. As a result, it has been found that the degradation efficiency significantly reduced to 34.2%. Thus, the results reveal that the photocatalytic activities are strongly dependent on the $O_2^{\bullet-}$ radical which plays a crucial role in the decomposition of MB pollutant dye.

For optimization of the photocatalyst, the reproducibility of the results after reuse is an important parameter. The reusability of SrO has been tested for the decomposition of MB dye by repeating the experiment four times under irradiation with visible light. After each cycle of the experiment the SrO catalyst was separated from the solution through centrifugation and at the initiation of every experiment the concentration of dye was set to its initial value. The values of the obtained degradation efficiency are 87.4, 82.73, 73.25, and 68.1% corresponding to the four cycles, suggesting that the synthesized sample can be reused for photocatalysis. The slight loss of photo-degradation efficiency observed after each cycle of the experiment may be due to mechanical or experimental loss of SrO nanoparticles during the photocatalytic process. In addition, due to the bonding affinity between the SrO catalyst and dye molecules, a certain quantity of dye resides on the catalyst surface after each catalytic cycle. The dye residue may cause a lessening of the adsorption of dye in the next cycle which causes a loss in photo-degradation efficiency.

Many research groups have reported the photocatalytic activity of various metal oxide nanoparticles.[45–53] The present work has been compared with the literature to measure the advantages of this work as shown in Table 1. It is observed from the table that *Albizia julibrissin* mediated SrO nanoparticles achieved an enhanced efficiency for the degradation of MB dye molecules under exposure to visible light irradiation compared with other metal oxides.

Conclusions

An additive-free SrO nanomaterial has been synthesized using plant extract as an effective resource for the synthesis of the material. The method is more accessible and environmentally friendly in comparison to other traditional methods. The plant extract has been found to be an efficient capping and stabilizing agent that is responsible for controlling particle size, morphology, structure and other characteristic features of the synthesized material. XRD results confirmed the structure of SrO nanoparticles, whereas FESEM and TEM studies revealed the spherical morphology of the synthesized SrO nanoparticles and their diameter was observed to be in the range of 20–30 nm. EDX analysis and mapping substantiate the higher amount of Sr than O element, with weight percentages of 67.2 and 32.8% of the total weight, respectively. The results of FTIR and XPS are analogous to each other and showed the presence of phyto-constituents which assist the formation of SrO NPs. The energy bandgap is an important parameter for the photocatalytic activity and has been estimated (2.64 eV) from the UV-DRS spectrum through a Tauc plot. The photocatalytic response of SrO nanoparticles has been tested against the degradation of MB dye under visible light irradiation. The photo-degradation efficiency of 87.4% and pseudo-first-order reaction rate constant of 0.23 min^{-1} indicate that the SrO nanoparticles act as an efficient and active photocatalyst. The photo-degradation efficiency is found to be mainly contributed by $O_2^{\bullet -}$ radicals, as shown by scavenging experiments. After the 4^{th} cycle of the experiment with the same SrO photocatalyst, the efficiency is 68.1%, showing its capacity for reuse and potential for commercial use.

From this study, we recommend an eco-friendly *Albizia julibrissin* mediated SrO photocatalyst prepared *via* a green synthesis method with enhanced photocatalytic activity under eco-friendly conditions, *i.e.* under visible light irradiation. From the results, it is observed that SrO can be used to treat cationic dye pollutants dissolved in water.

Conflicts of interest

There are no conflicts to declare.

Acknowledgements

The authors are thankful to the Athmic Biotech Lab, Kaliyoor, Kerala for providing research facilities.

References

1 M. A. Vélez, M. C. Perotti, L. Santiago, A. M. Gennaro and E. Hynes, Bioactive compounds delivery using nanotechnology: design and applications in dairy food, in *Nutrient Delivery*, Elsevier, 2017. pp. 221–250.
2 A. Bera and H. Belhaj, Application of nanotechnology by means of nanoparticles and nanodispersions in oil recovery – a comprehensive review, *J. Nat. Gas Sci. Eng.*, 2016, **34**, 1284–1309.
3 M. Wainwright, Dyes in the development of drugs and pharmaceuticals, *Dyes Pigm.*, 2008, **76**, 582–589.
4 K. Yamjala, M. S. Nainar and N. R. Ramisetti, Methods for the analysis of azo dyes employed in food industry – a review, *Food Chem.*, 2016, **192**, 813–824.
5 A. Cruz-Rizo, S. Gutiérrez-Granados, R. Salazar and J. M. Peralta-Hernández, Application of electro-Fenton/BDD process for treating tannery wastewaters with industrial dyes, *Sep. Purif. Technol.*, 2017, **172**, 296–302.
6 F. Mashkoor and A. Nasar, Magsorbents: potential candidates in wastewater treatment technology – a review on the removal of methylene blue dye, *J. Magn. Magn. Mater.*, 2020, **500**, 166408.
7 G. K. Sarma, S. Sen Gupta and K. G. Bhattacharyya, Removal of hazardous basic dyes from aqueous solution by adsorption onto kaolinite and acid-treated kaolinite: kinetics, isotherm and mechanistic study, *SN Appl. Sci.*, 2019, **1**, 211.
8 T. Cheng, H. Gao, G. Liu, Z. Pu, S. Wang, Z. Yi, X. Wu and H. Yang, Preparation of core–shell heterojunction photocatalysts by coating CdS nanoparticles onto $Bi_4Ti_3O_{12}$ hierarchical microspheres and their photocatalytic removal of organic pollutants and Cr(VI) ions, *Colloids Surf., A*, 2022, **633**, 127918.
9 S. Shakoor and A. Nasar, Adsorptive decontamination of synthetic wastewater containing crystal violet dye by employing *Terminalia arjuna* sawdust waste, *Groundw. Sustain. Dev.*, 2018, **7**, 30–38.

10 M. A. Brown and S. C. De Vito, Predicting azo dye toxicity, *Crit. Rev. Environ. Sci. Technol.*, 1993, **23**, 249–324.
11 R. Ye, M. Zhao, X. Mao, Z. Wang, D. A. Garzón, H. Pu, Z. Zhao and P. Chen, Nanoscale cooperative adsorption for materials control, *Nat. Commun.*, 2021, **12**, 1–9.
12 B. Liu, J. Ji, B. Zhang, W. Huang, Y. Gan, D. Y. C. Leung and H. Huang, Catalytic ozonation of VOCs at low temperature: a comprehensive review, *J. Hazard. Mater.*, 2022, **422**, 126847.
13 S. K. Bhagat, T. M. Tung and Z. M. Yaseen, Heavy metal contamination prediction using ensemble model: case study of Bay sedimentation, Australia, *J. Hazard. Mater.*, 2021, **403**, 123492.
14 T. Cheng, H. Gao, R. Li, S. Wang, Z. Yi and H. Yang, Flexoelectricity-induced enhancement in carrier separation and photocatalytic activity of a photocatalyst, *Appl. Surf. Sci.*, 2021, **566**, 150669.
15 Z. He, H. Yang, J. Su, Y. Xia, X. Fu, L. Kang, L. Wang and M. Wu, Polyacrylamide gel synthesis and photocatalytic performance of $CuCo_2O_4$ nanoparticles, *Mater. Lett.*, 2021, **288**, 129375.
16 L. Di, X. Sun, T. Xian, H. Li, Y. Gao and H. Yang, Preparation of Z-scheme Au-Ag_2S/Bi_2O_3 composite by selective deposition method and its improved photocatalytic degradation and reduction activity, *Adv. Powder Technol.*, 2021, **32**, 3672–3688.
17 S. Tang, Z. Fu, Y. Li and Y. Li, Study on boron and fluorine-doped C_3N_4 as a solid activator for cyclohexane oxidation with H_2O_2 catalyzed by 8-quinolinolato iron^{III} complexes under visible light irradiation, *Appl. Catal., A*, 2020, **590**, 117342.
18 T. Xian, X. Sun, L. Di, H. Li and H. Yang, Improved photocatalytic degradation and reduction performance of Bi_2O_3 by the decoration of AuPt alloy nanoparticles, *Opt. Mater.*, 2021, **111**, 110614.
19 X. Chen, Y. Zhou, H. Han, X. Wang, L. Zhou, Z. Yi, Z. Fu, X. Wu, G. Li and L. Zeng, Optical and magnetic properties of small-size core–shell Fe_3O_4@C nanoparticles, *Mater. Today Chem.*, 2021, **22**, 100556.
20 Z. Zheng, X. Zu, Y. Zhang and W. Zhou, Rational design of type-II nano-heterojunctions for nanoscale optoelectronics, *Mater. Today Phys.*, 2020, **15**, 100262.
21 A. Mehta, A. Mishra, S. Basu, N. P. Shetti, K. R. Reddy, T. A. Saleh and T. M. Aminabhavi, Band gap tuning and surface modification of carbon dots for sustainable environmental remediation and photocatalytic hydrogen production – a review, *J. Environ. Manage.*, 2019, **250**, 109486.
22 S. Rohilla, A. Gupta, V. Kumar, S. Kumari, M. Petru, N. Amor, M. T. Noman and J. Dalal, Excellent UV-light triggered photocatalytic performance of ZnO SiO_2 nanocomposite for water pollutant compound methyl orange dye, *Nanomaterials*, 2021, **11**, 2548.
23 R. M. Mohamed and A. A. Ismail, Photocatalytic reduction and removal of mercury ions over mesoporous CuO/ZnO S-scheme heterojunction photocatalyst, *Ceram. Int.*, 2021, **47**, 9659–9667.
24 Z. Huang, X. Zhao, H. Xia, F. Lu, L. Hu and P. K. Chu, Insights into enhancement of photocatalytic properties of g-C_3N_4 by local electric field induced by polarization of MgO(111), *J. Environ. Chem. Eng.*, 2021, **9**, 105922.
25 A. A. Fauzi, A. A. Jalil, N. S. Hassan, F. F. A. Aziz, M. S. Azami, I. Hussain, R. Saravanan and D. V. Vo, A critical review on relationship of CeO_2-based photocatalyst towards mechanistic degradation of organic pollutant, *Chemosphere*, 2022, **286**, 131651.
26 D. Li, J. Huang, R. Li, P. Chen, D. Chen, M. Cai, H. Liu, Y. Feng, W. Lv and G. Liu, Synthesis of a carbon dots modified g-C_3N_4/SnO_2 Z-scheme photocatalyst with superior photocatalytic activity for PPCPs degradation under visible light irradiation, *J. Hazard. Mater.*, 2021, **401**, 123257.
27 T. Soltani, X. Zhu, A. Yamamoto, S. P. Singh, E. Fudo, A. Tanaka, H. Kominami and H. Yoshida, Effect of transition metal oxide cocatalyst on the photocatalytic activity of Ag loaded $CaTiO_3$ for CO_2 reduction with water and water splitting, *Appl. Catal., B*, 2021, **286**, 119899.
28 T. Li, A. Abdelhaleem, W. Chu, S. Pu, F. Qi and J. Zou, S-doped TiO_2 photocatalyst for visible LED mediated oxone activation: Kinetics and mechanism study for the photocatalytic degradation of pyrimethanil fungicide, *Chem. Eng. J.*, 2021, **411**, 128450.
29 P. Anbu, S. C. B. Gopinath, M. N. Salimi, I. Letchumanan and S. Subramaniam, Green synthesized strontium oxide nanoparticles by *Elodea canadensis* extract and their antibacterial activity, *J. Nanostruct. Chem.*, 2021, 1–9.
30 C. S. Lau, D. J. Carrier, R. R. Beitle, D. I. Bransby, L. R. Howard, J. O. Lay Jr, R. Liyanage and E. C. Clausen, Identification and quantification of glycoside flavonoids in the energy crop *Albizia julibrissin*, *Bioresour. Technol.*, 2007, **98**, 429–435.
31 I. Nehdi, Characteristics, chemical composition and utilisation of *Albizia julibrissin* seed oil, *Ind. Crops Prod.*, 2011, **33**, 30–34.
32 A. A. Gungor, H. Nadaroglu and D. D. Gultekin, Synthesis and Characterization of Nano-Strontium Oxide (SrO) Using Erzincan Cimin Grape (*Vitis vinifera*, Cimin), *Chem. Sci. Int. J.*, 2019, 1–7.
33 G. Apsana, P. P. George, N. Devanna and R. Yuvasravana, Biomimetic synthesis and antibacterial properties of strontium oxide nanoparticles using *Ocimum sanctum* leaf extract, *Asian J. Pharm. Clin. Res.*, 2018, **11**, 384–389.
34 V. V Makarov, A. J. Love, O. V Sinitsyna, S. S. Makarova, I. V Yaminsky, M. E. Taliansky and N. O. Kalinina, "Green" nanotechnologies: synthesis of metal nanoparticles using plants, *Acta Naturae*, 2014, **6**, 35–44.
35 V. Arya, Living Systems: eco-friendly nanofactories, *Dig. J. Nanomater. Biostructures*, 2010, **5**, 9.
36 M. Naseer, U. Aslam, B. Khalid and B. Chen, Green route to synthesize Zinc Oxide Nanoparticles using leaf extracts of *Cassia fistula* and *Melia azadarach* and their antibacterial potential, *Sci. Rep.*, 2020, **10**, 1–10.

37 T. Ikeda, S. Fujiwara, K. Araki, J. Kinjo, T. Nohara and T. Miyoshi, Cytotoxic glycosides from *Albizia julibrissin*, *J. Nat. Prod.*, 1997, **60**, 102–107.

38 V. Adimule, S. S. Nandi, B. C. Yallur, D. Bhowmik and A. H. Jagadeesha, Optical, Structural and Photoluminescence Properties of Gd*x*SrO:CdO Nanostructures Synthesized by Co Precipitation Method, *J. Fluoresc.*, 2021, **31**, 487–499.

39 S. Nsanzamahoro, L. Li, F. P. Mutuyimana, J. Liu, C. Ren, H. Qin and H. Chen, Synthesis of fluorescent and water-soluble silicon nanoparticles with a high pH response and its application to pH measurement and gastric parietal cell imaging, *New J. Chem.*, 2020, **44**, 19294–19299.

40 V. Karthick, V. G. Kumar, T. S. Dhas, K. Govindaraju, S. Sinha and G. Singaravelu, Biosynthesis of gold nanoparticles and identification of capping agent using gas chromatography-mass spectrometry and matrix assisted laser desorption ionization-mass spectrometry, *J. Nanosci. Nanotechnol.*, 2015, **15**, 4052–4057.

41 D. Kılıç, M. Sevim, Z. Eroğlu, Ö. Metin and S. Karaca, Strontium oxide modified mesoporous graphitic carbon nitride/titanium dioxide nanocomposites (SrO-mpg-CN/TiO_2) as efficient heterojunction photocatalysts for the degradation of tetracycline in water, *Adv. Powder Technol.*, 2021, **32**, 2743–2757.

42 M. M. Rahman, M. M. Alam, A. M. Asiri, K. A. Alamry and M. A. Hasnat, Facile SrO nanorods: an efficient and alternate detection approach for the selective removal of 4-aminophenol towards environmental safety, *New J. Chem.*, 2020, **44**, 15507–15514.

43 M. M. Rahman, M. M. Hussain and A. M. Asiri, A novel approach towards hydrazine sensor development using SrO·CNT nanocomposites, *RSC Adv.*, 2016, **6**, 65338–65348.

44 V. V Atuchin, V. G. Kesler, A. I. Zaitsev, M. S. Molokeev, A. S. Aleksandrovsky, A. A. Kuzubov and N. Y. Ignatova, Electronic structure of α-SrB_4O_7: experiment and theory, *J. Phys.: Condens. Matter*, 2013, **25**, 85503.

45 R. C. Hatch, K. D. Fredrickson, M. Choi, C. Lin, H. Seo, A. B. Posadas and A. A. Demkov, Surface electronic structure for various surface preparations of Nb-doped $SrTiO_3$ (001), *J. Appl. Phys.*, 2013, **114**, 103710.

46 V. V Atuchin, J. C. Grivel and Z. Zhang, Core level photoemission spectroscopy and chemical bonding in $Sr_2Ta_2O_7$, *Chem. Phys.*, 2009, **360**, 74–78.

47 U. Alam, A. Khan, D. Ali, D. Bahnemann and M. Muneer, Comparative photocatalytic activity of sol–gel derived rare earth metal (La, Nd, Sm and Dy)-doped ZnO photocatalysts for degradation of dyes, *RSC Adv.*, 2018, **8**, 17582–17594.

48 K. R. Nemade and S. A. Waghuley, UV-vis spectroscopic study of one pot synthesized strontium oxide quantum dots, *Results Phys.*, 2013, **3**, 52–54.

49 Y. Zhang, L. Deng, G. Zhang and H. Gan, Facile synthesis and photocatalytic property of bicrystalline TiO_2/rectorite composites, *Colloids Surf., A*, 2011, **384**, 137–144.

50 Y. Guo, G. Zhang, J. Liu and Y. Zhang, Hierarchically structured α-Fe_2O_3/Bi_2WO_6 composite for photocatalytic degradation of organic contaminants under visible light irradiation, *RSC Adv.*, 2013, **3**, 2963–2970.

51 S. Harish, M. Navaneethan, J. Archana, A. Silambarasan, S. Ponnusamy, C. Muthamizhchelvan and Y. Hayakawa, Controlled synthesis of organic ligand passivated ZnOnanostructures and their photocatalytic activity under visible light irradiation, *Dalton Trans.*, 2015, **44**, 10490–10498.

52 B. Subash, B. Krishnakumar, R. Velmurugan, M. Swaminathan and M. Shanthi, Synthesis of Ce co-doped Ag-ZnO photocatalyst with excellent performance for NBB dye degradation under natural sunlight illumination, *Catal. Sci. Technol.*, 2012, **2**, 2319–2326.

53 Y. Zhang, H. Gan and G. Zhang, A novel mixed-phase TiO_2/kaolinite composites and their photocatalytic activity for degradation of organic contaminants, *Chem. Eng. J.*, 2011, **172**, 936–943.

54 K. Vignesh, M. Rajarajan and A. Suganthi, Visible light assisted photocatalytic performance of Ni and Th co-doped ZnO nanoparticles for the degradation of methylene blue dye, *J. Ind. Eng. Chem.*, 2014, **20**, 3826–3833.

55 P. Velusamy and G. Lakshmi, Enhanced photocatalytic performance of (ZnO/CeO_2)-β-CD system for the effective decolorization of Rhodamine B under UV light irradiation, *Appl. Water Sci.*, 2017, **7**, 4025–4036.

56 S. P. Kim, M. Y. Choi and H. C. Choi, Photocatalytic activity of SnO_2 nanoparticles in methylene blue degradation, *Mater. Res. Bull.*, 2016, **74**, 85–89.

57 T. Bhuyan, K. Mishra, M. Khanuja, R. Prasad and A. Varma, Biosynthesis of zinc oxide nanoparticles from *Azadirachta indica* for antibacterial and photocatalytic applications, *Mater. Sci. Semicond. Process.*, 2015, **32**, 55–61.

58 R. M. Tripathi, A. S. Bhadwal, R. K. Gupta, P. Singh, A. Shrivastav and B. R. Shrivastav, ZnO nanoflowers: Novel biogenic synthesis and enhanced photocatalytic activity, *J. Photochem. Photobiol., B*, 2014, **141**, 288–295.

59 Y. Zheng, L. Fu, F. Han, A. Wang, W. Cai, J. Yu, J. Yang and F. Peng, Green biosynthesis and characterization of zinc oxide nanoparticles using *Corymbia citriodora* leaf extract and their photocatalytic activity, *Green Chem. Lett. Rev.*, 2015, **8**, 59–63.

60 M. I. Khan, M. N. Akhtar, N. Ashraf, J. Najeeb, H. Munir, T. I. Awan, M. B. Tahir and M. R. Kabli, Green synthesis of magnesium oxide nanoparticles using *Dalbergia sissoo* extract for photocatalytic activity and antibacterial efficacy, *Appl. Nanosci.*, 2020, **10**, 2351–2364.

61 H. L. Tu, Biosynthesis, Characterization and Photocatalytic Activity of Copper/Copper Oxide Nanoparticles Produced Using Aqueous Extract of Lemongrass Leaf, *Compos. Mater.*, 2019, **3**, 30–35.

62 J. Osuntokun, D. C. Onwudiwe and E. E. Ebenso, Green synthesis of ZnO nanoparticles using aqueous *Brassica oleracea* L. var. *italica* and the photocatalytic activity, *Green Chem. Lett. Rev.*, 2019, **12**, 444–457.

63 S. Sathishkumar, M. Parthibavarman, V. Sharmila and M. Karthik, A facile and one step synthesis of large surface

area SnO_2 nanorods and its photocatalytic activity, *J. Mater. Sci.: Mater. Electron.*, 2017, **28**, 8192–8196.

64 J. Sackey, A. K. H. Bashir, A. E. Ameh, M. Nkosi, C. Kaonga and M. Maaza, Date pits extracts assisted synthesis of magnesium oxides nanoparticles and its application towards the photocatalytic degradation of methylene blue, *J. King Saud Univ., Sci.*, 2020, **32**, 2767–2776.